Effects of planetary radius contraction on scattering

Viktor Hrannar Jónsson

Lund Observatory
Lund University

2020-EXA166

Degree project of 15 higher education credits
June 2020

Supervisor: Alexander Mustill

Lund Observatory
Box 43
SE-221 00 Lund
Sweden

Abstract

The observed high orbital eccentricities of many giant exoplanets is thought to be the result of gravitational scattering between planets. Outcomes of planet-planet scattering can result in some planets being lost by ejections into interstellar space, or collisions between planets or with the star. The likelihood of collisions for a planet with a certain mass, increases with larger radii. After planets have been formed they will then cool and contract, which probably affects the rate of collisions and the evolution of planetary orbits.

The purpose of this thesis is to examine how planetary contraction affects the outcomes of planet-planet scattering. By the use of numerical simulations I analyze of the outcomes of three $1M_J$ planet systems with fixed $1R_J$, $1.5R_J$, $2R_J$ radii, as well as a changing radii that follows a contraction curve from a cooling model for giant planets based on general cooling theory of Brown Dwarfs.

The results show that larger planetary radii indeed lead to more collisions, which in turn produces lower final eccentricity distributions. While the timescales for collisions remained the same as for the fixed radii, more collisions occurred earlier within that time-frame for the changing radii systems. The use of present-day radii underestimates the rate of collisions, which planetary systems with contracting radii giants otherwise experience. The cumulative eccentricity distribution for simulations with changing radii also showed lower final eccentricities, as expected from the increased collision rate. Although the $2R_J$ set showed similar amounts of collisions and ejections as the changing radii simulation, the final eccentricity distribution differed significantly. Perhaps suggesting that the time dependence of the collision rate has an effect on planetary orbital evolution.

Populärvetenskaplig beskrivning

Sedan den första bekräftade upptäckten av planeter utanfört vårat solsystem år 1992 har över 4000 fler hittats. Den data man har kunnat samlat ger ett gott underlag till att jämföra med resultaten av datorsimuleringar, i hopp om att bättre kunna förstå hur planetsystem formas och utvecklas.

Planeter formas i en såkallad protoplanetär skiva, bestående av 1% stoft och 99% gas, som roterar runt en ung stjärna. Gasen i skivan ger uppstånd till motstånd som förhindrar planeternas omloppsbanor från att ändras markant. Efter att gasen försvinner börjar sedan en utveckling i omloppsbanorna då planeterna gravitationellt interagera med varandra. Nyformade planeter har en hög mängd värme som dem sedan strålar bort, vilket innebär att planeten kyls ner över sin livstid. I fallet av gasplaneter innebär nerkylningen också att den tjocka atmosfären ökar i densitet, och att planeten i helhet blir mindre.

Bland dem observerade planeterna kan man märka att många jätteplaneter har betydligt mer ovala banor än gasjättarna i solsystemet. Denna höga excentricitet tror man är en produkt av gravitationella interaktioner när planeter möts på nära håll, då planeter även kan komma att kollidera med varandra eller kastas ut ur planetsystemet. Med numeriska simulationer har forskare kunnat studera hur excentricitetsfördelningar påverkas av interaktionerna, och jämfört med observationell data.

Förutom planeternas massa så har även radien en roll i hur planeter försvinner ur systemet. Det här arbetet har som ändamål att utforska effekten som sammandragningen av gasjättar kan ha på utvecklingen av planeternas omloppsbanor. Resultaten från numeriska simulationer ska hjälpa med att besvara skillnaden på hur planeter förloras, samt den slutliga excentricitets fördelningen.

Contents

List of Figures

List of Tables

Chapter 1

Introduction

The first confirmed planets orbiting another star were published by Wolszczan and Frail (1992). They were terrestrial sized, and orbited a pulsar. Only three years later Michel Mayor and Queloz (1995) first detected an exoplanet around a main sequence star, for which they were awarded the Nobel Prize in physics in 2019. In the last three decades exoplanetory research has developed greatly. Over 4000 planets have now been confirmed[1], giving context for our understanding of our own place in the universe.

Different methods of discovery and observation give different insights to features of the planet's orbit. One of the most successful methods is the transit method, which detects planets by the dimming of the star's light when the planet crosses in front of the star. Radial velocity is another common method, which measures the Doppler shift of certain spectral lines from a star, the star's moving caused by the planet exerting a gravitational pull on it as it orbits around. An exoplanet discovery is not considered to be confirmed with transit detection alone, as at that point it lacks a necessary mass estimate, which one can get from a subsequent radial velocity measurement.

So far, observations are still limited by the size of the planets. Using the transit method the planet must be physically wide enough to block a significantly measurable part of its host star, and for the radial velocity method the planets must be massive enough for the gravitational pull to be observable. Looking at the most current data from exoplanet databases shows that of the giant planets, many of them have high eccentricities. This is believed to be caused by planet-planet scattering. In which planets will, during close encounters, excite each others orbits. With a large enough gravitational kick a planet can get ejected out of the system, or if the distance between them gets sufficiently small they will collide.

Advancement in computational capabilities and the many new observations opens a door to research the evolution of planetary orbital dynamics. In which large sets of simulations can be performed using n-body integrators, then comparing the results to the set of confirmed observed exoplanets.

Planets are formed around young stars in so called protoplanetary disks. The disks

[1] http://exoplanet.eu/catalog/ - Accessed: May 5th 2020

consist of 99% gas and 1% dust, rotating around the star on a flat plane. During formation the protoplanets are subject to drag from the gas which dampens most orbital excitation that would otherwise occur from gravitational interactions between planets. Eventually, after a few million years, the gas disappears from the disc allowing for the planetary orbits to evolve freely without the drag from the gas dampening any orbital excitations. It is during this post-gas stage that most orbital evolution is understood to happen. Under periods of instability the planets can undergo close encounters where they can collide, scatter off each other into more eccentric orbits, or even be ejected from the system entirely.

Up until now research into planet-planet scattering has been done under the simplification of constant planet density. However, the density is in fact a temperature dependent function. Meaning that as giant planets with large gas envelopes cool down after formation, they will also increase in density and thus contract. Terrestrial planets, such as Earth, are not as susceptible to significant density changes as they cool down due to them being mostly only the rocky core. Due to the planetary radii being an important factor in determining the fallout of close encounters, such as collisions being dependent on the planets cross section, this project sets out to look at how contracting planets differ from fixed cool planets in these types of simulations.

The timescales for instabilities and when different types of events occur depend on the initial orbit parameters used for simulations as well as the planetary masses (Davies et al., 2014). Jurić and Tremaine (2008) performed sets of simulations with various initial conditions and number of planets, and found that collisions will be the dominant mode for planets to be lost on dynamical timescales, earlier on in the simulation times compared to ejections. A majority of planets lost were due to ejections, while collisions caused $3-20\%$ of planets to be lost. A portion of planets collided with the star, most often caused by more massive planets gradually exciting their eccentricities.

The aim of this project is to perform numerical simulations to investigate how the contraction of giant planets, after the dissipation of gas in the protoplanetary disk, may affect the rate of collisions and ejections. As well as studying the effects which this in turn has on the final eccentricity distribution of planets.

Chapter 2

Theory

2.1 Keplerian Orbital Elements

When working with orbits of planets, the Keplerian orbital elements are often preferred over the more common Cartesian coordinate system. In Cartesian coordinates, the orbits are described by the 3 dimensional position and velocity components, giving rise to six degrees of freedom in total. Keplerian orbital elements are developed from Kepler's first law, which states that planets orbit in elliptical paths where the host star is positioned in one of the ellipse's focal points. Such that the six degrees of freedom are instead determined by the shape and orientation of an ellipse. The Keplerian elements are depicted in figure 2.1, and we consider the position of the star to be the space's origin.

The semi-major axis, a, is half the longest possible length between two points on the ellipse. The eccentricity, e, is a measure of how non-circular the orbit is. The zero-value for e indicates a perfect circle, higher values up to (but not including) 1 express how non-circular the ellipse becomes.

An orbital plane is spanned by the points on the ellipse and can be tilted from some reference direction, the tilt being measured by the inclination angle i. Where the orbit crosses the reference plane, spanned in part by the reference direction, in an upward direction is called the ascending node. So the longitude of the ascending node, Ω, is the angle between the position of the ascending node and the reference direction, and orients the orbital inclination.

The argument of perihelion, ω, then orients the eccentricity of the orbit on the orbital plane, as an angle between the perihelion and the ascending node. Lastly, the mean anomaly, M, determines where the planet is positioned on the orbit, in expressing the fraction of orbital period elapsed since passing through perihelion as an angle. In figure 2.1 the true anomaly ν is depicted instead of M, which is the true geometrical angle.

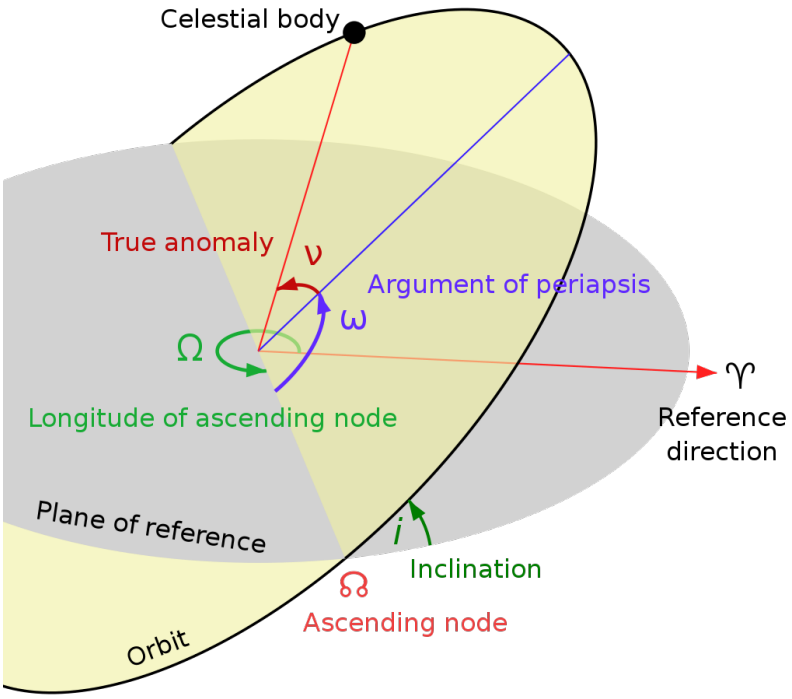

Figure 2.1: A depiction of the Keplerian orbital elements ν, ω, Ω and i which in part describe planetary orbits. Eccentricity e and semi-major axis a are not depicted. Wikimedia Commons (2007)

2.2 Formation of Planetary Systems

In this project we take a look at how the orbits of Jupiter-like gas giants can change when they cool and contract in the early stages of their lifetimes. Planets are formed in a protoplanetary disk surrounding newly formed stars. The flat disk consists of 99% gas and 1% dust in rotation around the star, which also slowly moves in towards the star. The disk disappears in part by accretion by the star, and after a few million years the radiation from the star has evaporated the remaining gas in a phenomenon called photoevaporation (Hogerheijde, 2011).

As presented in Jurić and Tremaine (2008), formation of planetary systems can be simplistically considered as happening in two stages. In the first stage planetary cores are formed through the fusion of smaller solid bodies, which in turn were formed by coagulation of dust particles in the protoplanetary disk. If the cores are massive enough, their gravitational pull could hold an envelope of gas around the core. In the second stage, the planetary system evolves by primarily gravitational interaction after gas has dissipated from the disk.

Armitage (2007) explains the core accretion model where cores of giant planets are formed in the same manner as for terrestrial planets, the difference being the eventual core mass being able to accrete and hold a large envelope of gas. The cores can grow by collisions of planetesimals (km sized), or perhaps more significantly by the accretion of pebbles. The core can continue to grow and eventually hold a significant envelope of gas around it. The growth of a planet by accreting gas stops either when a gap forms in the protoplanetary disk due to the planet itself, or when the gas in the disk has disappeared.

A prediction from the core accretion model is that eccentricities and inclinations of planets should be low (Winn and Fabrycky, 2015). The inclination being low due to the formation happening in a flat disk, and the planet eccentricities being low due to the streamlines being near-circular. As well as that any excitation in e or i will be counteracted by hydrodynamical drag with the disk.

2.2.1 Planet cooling

In Baraffe et al. (2003) the authors make a model to follow the cooling of extrasolar giant planets by applying general cooling theory for brown dwarfs. The model presented in the paper is based on the "COND" approach where dust opacity in the radiative transfer equation is neglected, and includes both irradiated and non-irradiated models.

For the purpose of this project the non-irradiated models will be used since the simulated planets are initially placed far enough away from the star to neglect irradiation. The irradiation however depends on the distance between the star and planet, which would imply for a system where orbits can change frantically during periods of instabilities, that the irradiation would vary over time. Within the scope of this project that could not be taken into consideration, and thus the neglecting of irradiation is a convenient simplification.

From Baraffe et al. (2003), a graph for the radius contraction of $1M_J$ planet was taken and fitted with a polynomial function. The graph displayed the contraction from 10^5 to

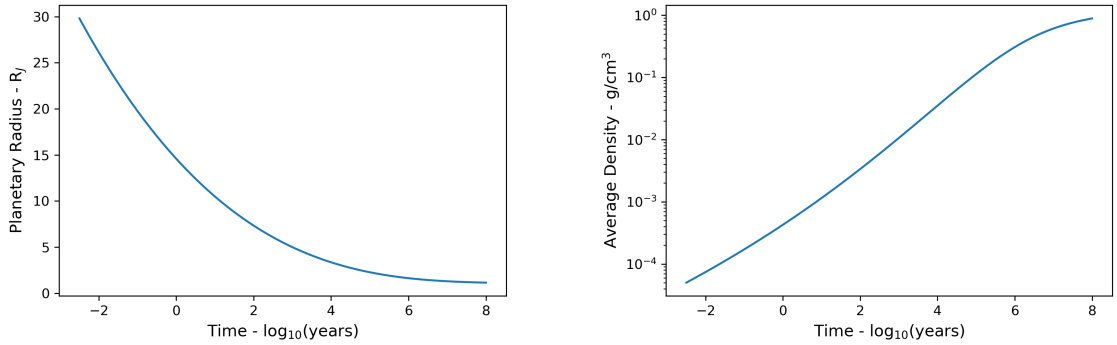

Figure 2.2: On the left, the 3rd degree polynomial fit for the changing planetary radius over time, of the result in Baraffe et al. (2003) for $1M_J$ planets. On the right, the equivalent change in average density over time.

10^9 years, and the purpose of the fit was to get a function for the radius over time which extends to earlier on in the contraction. Polynomial fits of the 2nd, 3rd and 4th degree were tried. The 2nd degree fit was to deemed to be too poor, while the 3rd and 4th degree fits were sufficiently accurate. Thus, the simpler 3rd degree fit would be used as the change in planetary radius over time for this project. Figure 2.2 shows the fitted path of the radius over time, as well as the equivalent change of the planets average density.

2.3 Planet-Planet Scattering

This section explains the events that can occur in the stage after the gas has dissipated from the protoplanetary disk, when gravitational interactions are the dominant force for planetary system evolution. The loss of a dampening force can lead to a growth in orbital eccentricities, which in turn can cause orbits to overlap and close encounters between planets. Scattering between planets could develop the high eccentricities which are seen for observed exoplanets (Chatterjee et al., 2008).

The timescales for instabilities will depend on the planetary masses and the initial separation. Low initial separations lead to earlier instabilities as the orbits are closer together, and higher masses have shorter instability timescales (Davies et al., 2014). The *Initial Separation Test* in section 4.2 explores the timescales of various initial separations to find which one fits the scope of this project.

Planet-planet scattering can also cause planets in the system to be lost. Those three types of events are: Collision between planets, planets being ejected from the system, and a planet colliding with the central body. The nature of these events differ such that the rate at which they happen will effect the final distributions of eccentricities.

The likelihood of a planet-planet collision depends on their respective cross sections, increasing with larger radii, and is independent of the masses. The Safronov number Θ is a helpful tool in assessing the outcomes of close encounters, defined in equation 2.1, where

M_p and R_p are the planet's mass and radius, M_* the stellar mass and a the semi-major axis. It is a quantification of a planets surface escape velocity compared to the planetary escape velocity at the planets semi-major axis. Small value Θ indicate an increased likelihood of collisions during close encounters.

$$\Theta^2 = \left(\frac{M_p}{M_*}\right)\left(\frac{R_p}{a}\right)^{-1} \tag{2.1}$$

Ejections can occur after close encounters between planets. An ejected planet is no longer gravitationally bound to the star it was formed around and thus considered to be lost from the planetary system. The surviving planet will feel a recoil from the event which can excite its eccentricity. Since the force is gravitational, the energy in the recoil will of course depend on the mass ratio between the two planets. In the scattering of unequal-mass planets, the more massive survivor is subject to a less energetic recoil then that of the survivors of an equal-mass event. Simply due to the fact that more energy is required for a planet to eject another planet of the same mass (Davies et al., 2014).

Chapter 3

Method

3.1 MERCURY

In this project, numerical simulations are performed using the n-body integrator software package `MERCURY6.2`, Chambers (1999). In our use it computes the motions of planets step-by-step, accounting for the gravitational pulls between all bodies in the simulation. Although the motions are calculated as for point masses, the integrator can account for collisions between the bodies using a set physical radii. `MERCURY` has a variate of integration algorithms to choose from, some of which are described briefly below.

One conventional algorithm used for the n-body integration of this type is Burlisch-Stoer (BS) and is available in `MERCURY`. Applied here it computes numerical solutions to the momentum of each body, as affected by the gravitational pull from all others. With the modified midpoint method each step in BS consists of multiple substeps, which are then used in a rational function extrapolation (Press et al., 1992). This is what allows the algorithm to have fairly large stepsizes without loosing too much in accuracy. The amount of substeps can be used to control the extrapolation errors. The estimated error is compared to the error of the same step performed with more substeps, if the fractional difference is below a specified tolerance parameter the integrator can move to the next step, if not, the extrapolation is reattempted with more substeps. For this project that tolerance parameter was set to 10^{-12}.

The Mixed-Variable Symplectic algorithm (MVS) is much faster in comparison with BS. MVS breaks up Hamilton's equations of motion such that the gravitational pull from the very massive central body can be 'built in' and separated from the pulls of smaller bodies (Chambers, 1999). The integrator then has to perform fewer computations in total, leading to lower run times for the simulations.

A characteristic of MVS is the fixed stepsize, necessary to preserve the Hamiltonian. During some events, such as close encounters between planets, the gravitational pull of the central body can lose its dominance relative to the gravitational forces exerted by the planets on each other. Meaning that the assumption made in how the equations of motion can be split-up faults and the integration error in each step increases significantly. One

remedy to retain accuracy is to momentarily decrease the integration step-size during such events, which however leads to a shift in the energy of the system. If it's necessary to change the step-size often in a single integration the errors will build up and the keplerian orbits can break down. MVS in this form is therefore not a suitable algorithm for the purpose of this project.

Chambers (1999) presents an integration algorithm which is an hybrid of MVS and BS. hereon referred to as the Hybrid algorithm. It ordinarily uses MVS, switching over to BS when planets are significantly close to each other. Thus it attempts to retain high accuracy from BS during close encounters, while harnessing the efficiency of MVS elsewhere. The change from one algorithm to another is done with a changeover function, allowing for a harmonious transition by 'fading out' one algorithm while the other emerges over some specified distance.

The accuracy of a simulation is determined by how well the integration has conserved both the energy and the angular momentum in the system. It is the total accumulated error estimated in each step of the integration. The total fractional change in energy due to the integration is therefore used to tell how accurate the simulation was, and require that it is below a 10^{-3} threshold to hold valid.

`MERCURY` considers bodies to have been ejected when their semi-major axis is greater then a set value, for this project that distance was set to 100 AU. It also has the ability to register close encounters, which occur when bodies come within a certain range of Hill radii (see eq. 3.1). For each integration step during the close encounter, `MERCURY` then checks if the bodies have collided by checking for an overlap of the physical radii. The exception being a collision with the central body, in which the collision is considered to have taken place if the smaller body has come within a distance of the origin, $1R_{\odot}$ in this project.

$$R_H = a\left(\frac{M_p}{3M_*}\right)^{1/3} \tag{3.1}$$

3.1.1 Dynamical Radii

In this project we want to see what effect a changing density has on planet-planet scattering and the final distribution of orbital parameters. For this purpose the physical planetary radii are based on the cooling curve of 1 M_J planets presented in chapter 2.2.1. In part by simulating various sets of planets with fixed radii and a set where the radii follows the fitted path, see figure 2.2.

For simulations with time dependent radii the BS algorithm, with variable timesteps, was used. A couple of new parts needed to be implemented into the subroutine `MAL_HVAR.FOR` in MERCURY which sees to it that the density is updated before it is applied in other parts of the subroutine for calculations. Below follows a bullet point description of `MAL_HVAR.FOR`, the new parts added for this project being marked with *(NEW)*.

- Initialization
  - Initialize some local variables

- *(NEW)* Change density, the pre-set value gets overwritten.
- Calculate close encounter limits and physical radii for bodies.
- Setup time for next output etc.

- Main Loop
  - Check if it's time for output or if the integration is finished.
  - Advance one timestep
  - *(NEW)* Update density
  - Check if close-encounters occurred
  - If collisions between planets or with the central body occurred: resolve it, remove lost object and recompute physical radii.
  - Check for ejections: remove lost objects

The way in which collisions are resolved has not been changed from the original code. Fragmentation is neglected, and the resulting body after the merge of two planets has their combined mass. The density is calculated in this method by using the mass of the body and the radius which changes over time. After a collision, the remaining planet then continuous to follow the same radius reduction curve.

3.2 Initial Parameter Generation

This section describes the initial values of orbital elements and fixed parameters set for the various simulated bodies. The central body was given Sun-like properties, with mass $1M_{\odot}$ and radius 0.005 AU.

All systems were run for three gas giants in the likes of Jupiter, with fixed mass $1M_J$. In `MERCURY` the size of planets is defined by the average density, and the radius then calculated from the density and mass. A radius of $1R_J$ corresponds to an average density of 1.33 g/cm^3 (Rothery et al., 2018). At places in this project where results from using different radii, the corresponding density is stated in connection.

As stated in section 2.1, the orbits of the planets are determined by 6 different parameters. The semi-major axes are chosen such that the inner planet is placed at 2 AU, and the remaining two subsequently placed at some separation. Which separation is most suitable for the scattering simulations is tested and determined in the section 4.2 *Initial Separation test*.

Like in the scattering experiments of Jurić and Tremaine (2008), we draw the initial value of eccentricities and inclination for the planets with the Rayleigh probability distribution, seen in equation 3.2 where σ is a scaling factor.

$$f(x, \sigma) = \frac{x}{\sigma^2} \exp\left(-x^2/(2\sigma^2)\right) \tag{3.2}$$

Ida and Makino (1992) showed through simulations that the relationship between the orbital inclination and eccentricity for a protoplanet has the dispersion $\langle e \rangle = 2\langle i \rangle$, where i are in units of radians. In this project the initial dispersion of these parameters are chosen such that the value of i, in radians, follows a Rayleigh distribution with $\sigma = 0.01$, and e is twice that value.

The three last parameters that orient the orbit are the argument of pericenter ω, the longitude of ascending node Ω, and the mean anomaly M. They are randomly set in the range $0° - 360°$ with a uniform distribution.

Chapter 4

Results

4.1 Typical Outcomes for Events

This section discusses some of the typical outcomes of scattering and showcases what they can look like in forms of orbital elements data over time. The results are taken from select systems in the Initial Separation test (section 4.2), where three $1M_J$ planets were simulated over 10^6 years. As such, the initial separation between example-cases vary.

Figure 4.1 shows the semi-major axis over time for a system where a collision between two planets occurs at roughly 40000 years. During a period of instability, ranging approximately from $2 \cdot 10^4$ years until the time of the collision, the outermost planet (Planet 3) gets moved much closer to the star. The others (Planet 1 and Planet 2) move outwards to orbits with larger a, and undergo frequent and continuous scattering ending in a collision between the two. After which the two remaining planets settle in stable orbits with final eccentricities $e_1 = 0.17$ and $e_3 = 0.35$.

Figure 4.2 shows two plots of the an ejection event occurring at approximately 12000 years. The left side plot shows a with respect to time for the three planets, while the right side plot shows the apses as well but only for the two outer planets (Planet 2 and Planet 3). Compared to the collision event, the planets in this case were initially separated much closer together, $\sim 0.6 - 0.7$ AU compared to $\sim 1 - 1.6$ AU. Early on in the simulation (10^2 years) the two outer planets begin to scatter. In the time 10^3 until the ejection event they collectively move outwards while the inner planet (Planet 1) proceeds to move closer to the star. Planet 3's eccentricity and orbits continuous to be excited, reaching $e > 0.9$ before the increasing semi-major axis finally is considered an ejection ($a > 100$ Au).

The final eccentricities for the ejection event case, after the two remaining planets who settled in stable orbits, were $e_1 = 0.72$ and $e_2 = 0.46$. A comparison with the collision case also showcases the effect mentioned in section 2.3, in which collision between planets tend to lead to more low eccentric survivors compared to ejections between equal-mass planets.

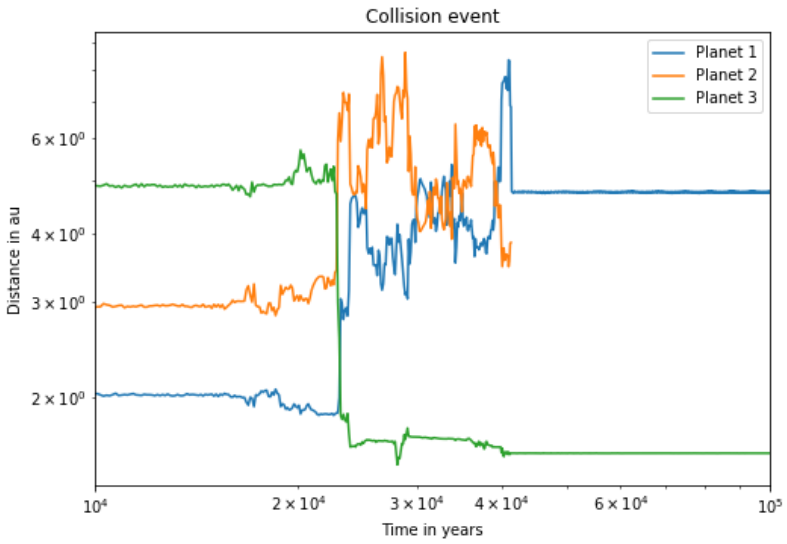

Figure 4.1: The semi-major axis for a system where two planets collide at 41000 years after a period of instability. Final eccentricities were $e_1 = 0.17$ and $e_3 = 0.35$

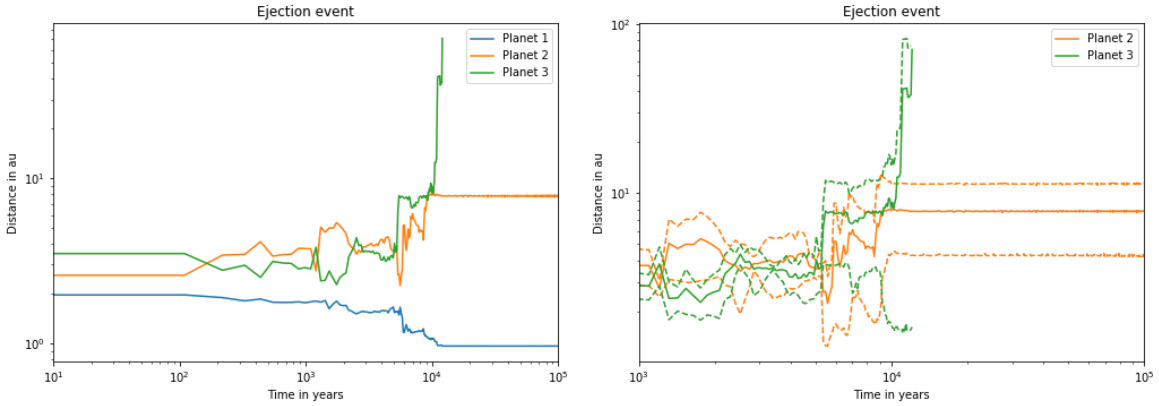

Figure 4.2: A system where a planet gets ejected ($a > 100$ AU), left image shows the semi-major axis over time. The image on the right more closely shows the interaction between Planet2 and Planet3 which leads to the ejection, where solid line is the semi-major axis and dashed lines are the apsis of the orbit.

4.2 Initial Separation Test

Chambers et al. (1996) found that systems with three or more planets, where planets were separated by $K < 10R_H$, where K is the difference in semi-major axes, were always unstable and that for time t, there existed a linear relation between $\log(t)$ of the first close encounter between planets and K.

$$\log(t) = a \cdot K + b \tag{4.1}$$

In this section we first try to replicate that result using our simulations and initial parameter generation. With that result, a reasonable initial separation of planets semi-major axes can also be determined for the subsequent simulations of fixed and dynamical radii.

This test involved running multiple systems with three planets at varying initial semi-major axis separation. The innermost planet was always placed at 2 AU. The second planet K-number of Hill radii, as defined in equation 3.1, from the first and the third planet at an equal number of Hill radii from the second. K varied from 2 to 8 R_H in steps of 0.2, three planetary systems were run for each step in K. The total of 93 systems, all had a simulation time of 10^6 years.

Out of the 93 systems, 49 had a fractional energy change due to integrator $> 10^{-3}$. Because those values are too high to deem the simulations accurate, they were subsequently rerun using the BS integrator instead of the hybrid integrator. After which all systems had $< 10^{-3}$ fractional energy change.

The graph in figure 4.3 shows the time of the first close encounters between planets in each system as blue crosses for each initial separation value K, in units of Hill Radii. A linear fit was made to the first encounter times, shown as the black line in figure 4.3. The coefficients of equation 4.1 for the fit are $a = 1.01378052$ and $b = -2.23665029$.

There are notable outliers among the first encounter times from the linearity, namely, the assortment of systems around $K \simeq 8R_H$. These systems have lower than expected times for the first close encounters. Upon further investigation, the middle planet in these systems turns out to be close to being, initially, in mean motion resonance with both the outer and inner planets where $\frac{P_i}{P_j} \simeq 2$. This synchronization of the orbits means that the orbits will evolve faster such that their eccentricities increase, which in turn allows for earlier first close encounters when the paths of planets overlap.

Figure 4.3 also includes the time at which planets collide or are ejected, as blue and orange dots respectively. It is apparent that in this test, ejections of planets into interstellar space tend to occur after 10^4 years, and that collisions between planets can happen as early as the first close encounters.

When determining what separation to use for integrations with fixed and changing radii, one must consider both the instability timescales and integration time limit. For separations between $2 - 4\ R_H$ the systems appear too unstable, with the first encounters and possible collisions occurring as early as during the first orbit. Separations above $7\ R_H$

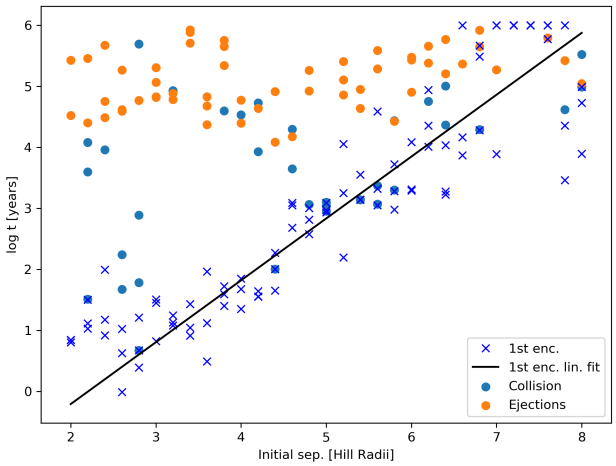

Figure 4.3: First close encounters (blue crosses) in each planetary systems compared to the initial semi-major axis separation in Hill radii, linearly fitted (black line). The systems marked at exactly 10^6 yrs did not have any close encounters between planets in the duration of the simulations. Collision and ejection events are marked as blue and orange solid circles respectively.

result in first encounters taking place too late in the limited integration time. This resulted in the choice of $K = 6R_H$ for the separation applied in the simulations presented in sections 4.4 and 4.5, where first encounters are expected on the order of $10^3 - 10^4$ years.

4.3 Integration Step Size Test

This section briefly tests the integration step sizes using the hybrid algorithm. The time to run simulations can be reduced if one can choose a larger step size. The larger step size should however not have significant impairment on the accuracy of the simulations. Thus, sizes of 4,6,12,25,50 days were tested, the larger end limited by 1/20th of the smallest initial orbital period (~ 51.7 days).

The graph in figure 4.4 shows resulting fractional energy change due to the integrator for 8 systems per chosen step size, drawing a minimum accuracy criteria at 10^{-3}. While all sizes have a few systems which fail the criteria, the fractional energy change for those who do get significantly lower with smaller sizes.

In reflection on the proportion of systems in the Initial Separation test (section 4.2) which also failed the criteria, with a step size of 8 days, fits in with the results of this test. When running integrations using the hybrid algorithm, systems that fail the accuracy criteria need to be rerun using the slower but more consistently accurate Burlisch-Stoer algorithm. If however up to half of the systems, or more, need to be rerun, the time ex-

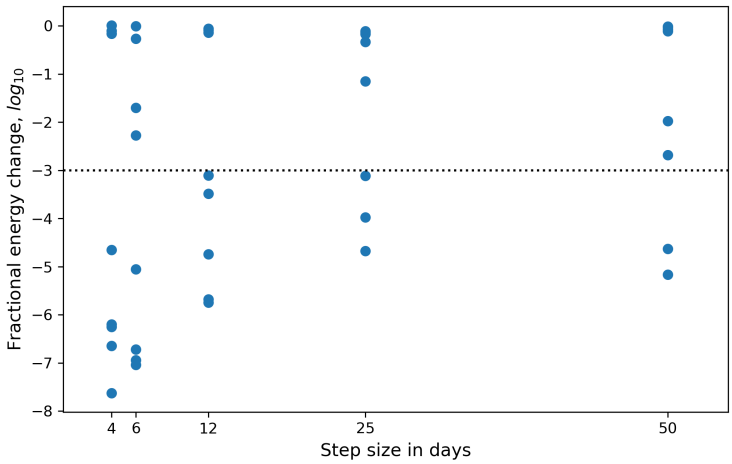

Figure 4.4: Fractional energy change of a set of 8 systems per tested integration step size. Simulating three $1M_J$ planets over 10^6 years using the hybrid algorithm.

pected to be saved by using the hybrid algorithm becomes indifferent. Out of convenience, the remaining integrations done in this project (i.e. section 4.4-4.5) were run using solely the BS algorithm with 10^{-12} error tolerance for each step.

4.4 Fixed Radii Runs

Performing simulations runs with fixed radii of various sizes can give a basic insight into what affect the radius might have on planet scattering and how planets are lost. It does not however give a full picture for the changing radii, as it might over- or underestimate some event types, which favor large radii.

To determine what radii to use for these sets, the original plot from Baraffe et al. (2003) was used, which the curve in figure 2.2 were based on. That plot had a lower limit of 10^5 years for the radius of a $1M_J$ planet. In the period between $10^5 - 10^6$ yrs the radii is on the interval of $2.2 - 1.5R_J$. Three sets of 100 planetary systems with three $1M_J$ planets, were what could be done within the scope of this project. Those three sets would each have different fixed radii of all planets; $1.5R_J$ and $2R_J$ which span the interval just mentioned, and $1R_J$ as a control sample to compare to. Table 4.1 shows the corresponding densities to the aforementioned radii. For all systems in the three sets the total fractional energy change due to the integrator was smaller than 10^{-4}, giving confidence in the accuracy of the simulations.

Figure 4.5 shows the rates for in what manner planets were lost in the different sets. The different sets had similar total planet losses: $1R_J/1.5R_J/2R_J$ losing 115/115/113 planets respectively out of 300. For increasing radius the balance between planet-planet collisions and ejections shifted, with collisions increasing for larger planetary radius, and ejections

Table 4.1: Radii and corresponding densities of Jupiter mass planets used in the fixed radii simulations.

R_J	ρ [g/cm^3]
1	1.33
1.5	0.393
2	0.166

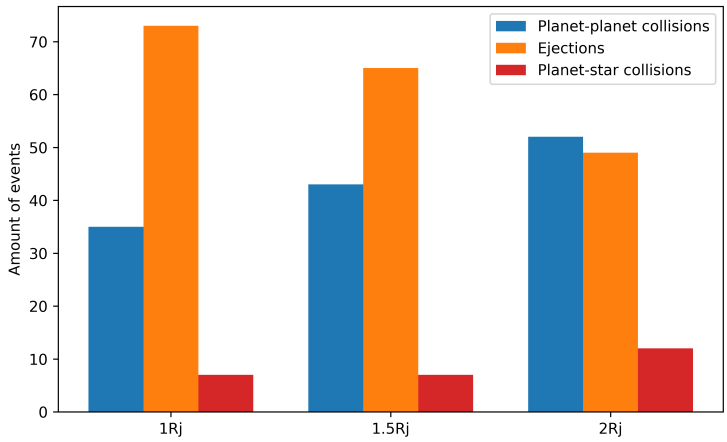

Figure 4.5: The amount of planets lost per event-type for the various fixed radii sets. Planet-planet collisions: 35/43/52, Ejections: 73/65/49, Collisions with star: 7/7/12, for 1RJ/1.5RJ/2RJ respectively.

decreasing. The number of times planets collided with the central body was small for all sets.

The timescales of when the different type of planet loss happens are shown in figure 4.6. As expected from the *initial separation test* in section 4.1, collisions begun to occur from the time of the first close encounters, around 10^3 years into the simulation. The median time for collisions is around 10^4 years, but they are present until almost the very end of the 10^6 year simulations. Ejections appear later on, with medians in the hundreds-of-thousands of years. The timescales for ejections and collisions respectively do not appear to be dependent on the size of the planetary radius, as they are similar for all three sets.

In figure 4.7, one can see the cumulative distribution of eccentricities for surviving planets at the end of simulation. The various radii sizes follow a closely similar distribution, where sets with larger radii have slightly more low-eccentric planets. A performed Kolmogorov-Smirnov test could however not conclude that the different integrated sets where not coming from the same distribution of eccentricities. In comparison with observational data[1] from similarly sized giants ($0.8 - 20M_J$) with orbital periods above 100

[1]http://exoplanet.eu/catalog/ - Accessed: April 14th 2020

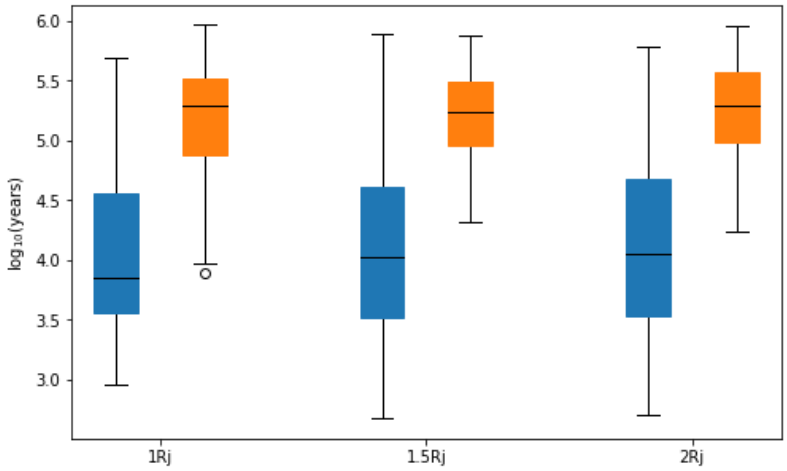

Figure 4.6: The time periods of collisions and ejections from the different fixed radii sets. Blue box and whiskers mark the range of times when collisions occurred, orange for ejections.

days, the simulations included more high eccentric planets.

4.5 Dynamical Radii Runs

This sections showcases the results from a set of 100 systems of three $1M_J$ planets each, where the planet radius contracts as described in section 2.2.1. `MERCURY` calculates the physical planetary radii from the density. But due to the nature of the fitting in section 2.2.1, the changing radii function diverges towards infinity at $t = 0$. Thus, during the integration initialization, the contraction curve needs to be offset from $t = 0$, such that it does not cause the simulation to break. For the simulations presented here, the offset was set to equal the 6 day integration step size which will have a negligible effect on the contraction in the long run. At $t = 6$ days the radius is $\sim 25R_J$, which is well within the Hill radii of the inner most planet (~ 0.1 AU) and will therefore not cause any breakage in the integration.

The fractional energy change due to the integrator was below 10^{-5} for all systems, which is deemed satisfactory.

The timescales for ejections and collisions are similar to the three sets of fixed radii, as can be seen in figure 4.8. However as indicated by the smaller box for collisions on the changing radii set, the earliest 3/4 of collisions had occurred $\sim$ 20000 years sooner than for the fixed radii simulations. For reference, the radii is $\sim 3.3R_J$ at 10^4 years. This shift towards earlier times for collision events can be reflected on with the Safronov number Θ, which quantifies likely outcomes of close encounters and is dependent on the planetary radius. Lower values favor collisions as an outcome of scattering, and figure 4.9 shows how Θ increases over time, as the radius contracts.

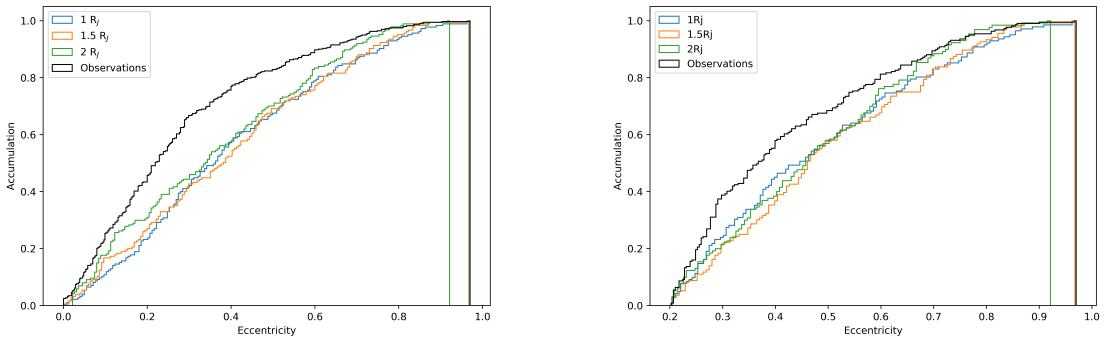

Figure 4.7: End of simulations cumulative eccentricity distribution for planets, compared to observational data. Figure on right only uses $e > 0.2$

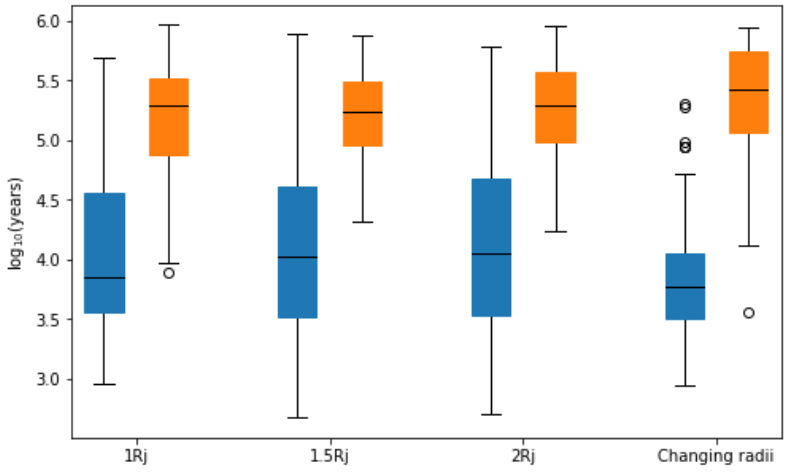

Figure 4.8: The time periods of collisions and ejections from the different fixed radii sets together with the changing radii set. Blue box and whiskers mark the range of times when collisions occurred, orange for ejections.

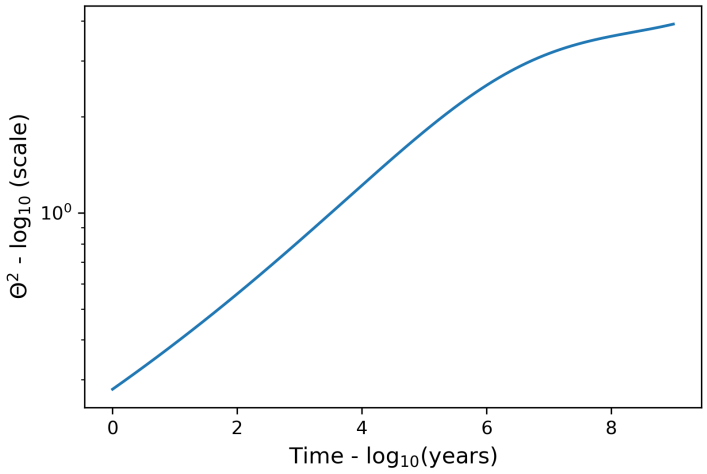

Figure 4.9: The Safronov number (eq. 2.1) for the $1M_J$ radius contraction in 2.2, at the initial placement of the inner planet $a = 2$ AU.

Out of the 300 initial planets 111 were lost to planet-planet collisions, ejections or collisions with the central body. The bar graph in figure 4.10 shows the distribution of this, in comparison to the sets of fixed radii systems. Collisions occurred slightly more often than ejections, in a similar amount and ratio as the set of $2R_J$ fixed radii planets, which is also significantly different from the $1R_J$ fixed radii control sample. Planets colliding with the central body are few, like for the fixed radii runs. All 100 systems lost at least one planet, of which 11 systems lost two.

The cumulative eccentricity distribution for this set of simulations is shown in figure 4.11, in comparison to both observational data and the fixed radii sets. The distribution is similar to that of the observational data at low eccentricities (< 0.2) but deviates from it for higher eccentricities where it more closely resembles the results of the fixed radii simulations. Notably the eccentricities differ between the changing radii set and the $2R_J$ fixed radii set, despite the similarity in the rate of collisions and ejections. A Kolmogorov-Smirnov test between the two, gives a p-value < 0.003 indicating that they are not drawn from the same distribution. The only other measured difference between the sets in this project was that collisions occurred more early on in the changing radii set. Perhaps suggesting that the final eccentricity distribution in addition to the dependence on the rate of collision, also depends on the time at which collisions occur.

Figure 4.12 shows a density plot for the final eccentricity of planets in systems where a collision occurred in comparison to systems without any collisions. It also shows the density of eccentricities for all surviving planets in the entire set. The plot shows that planets in systems where a collision took place have lower final eccentricities then the rest. If a collision is the first event where a planet is lost in a system, the two remaining planets will have unequal masses. As reviewed in Davies et al. (2014), scattering between unequal-mass planets have been shown to result in less eccentric distributions then scattering of

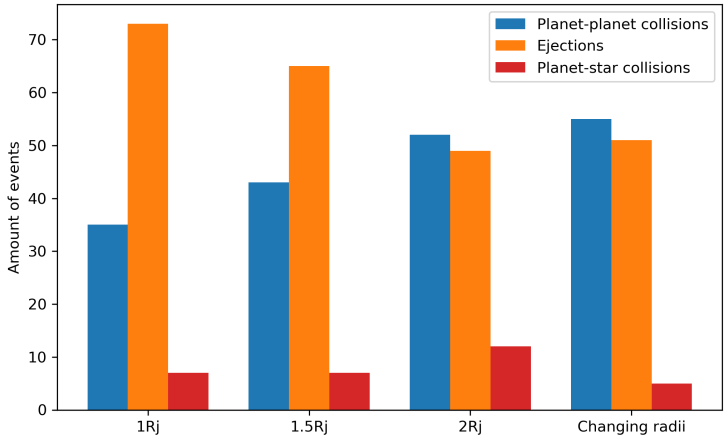

Figure 4.10: The amount of planetary losses per event-type, for the various fixed radii sets and the changing radii set. Planet-planet collisions: 35/43/52/55, Ejections: 73/65/49/51, Collisions with star: 7/7/12/5, for $1R_J/1.5R_J/2R_J$/changing radii respectively.

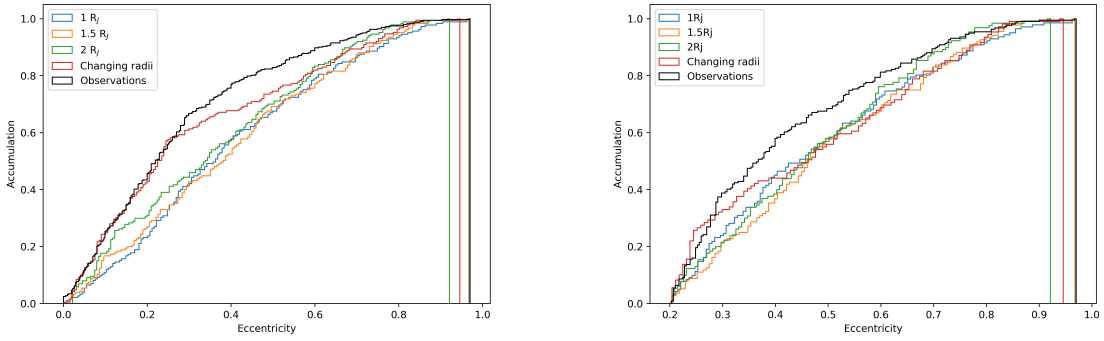

Figure 4.11: End of simulations cumulative eccentricity distribution for planets from the changing radii set, compared to observational data. Right hand side plot shows the same distribution limited to $e > 0.2$.

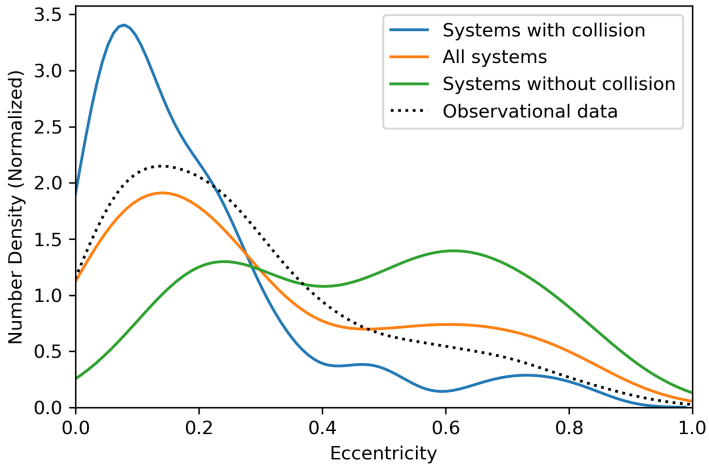

Figure 4.12: Density plots of eccentricities for planets in systems where: collision occurred, no collision occurred, and all systems are included respectively. Additionally, the dotted black line is the density of eccentricities for observed giant planets.

equal-mass planets.

The same deviation from the observational data in figure 4.11, is seen in figure 4.12 where the density of the whole set decreases into a plateau between eccentricities $0.4 - 0.8$, while the observational data continuous to decrease.

Finally, figure 4.13 shows the final eccentricities plotted against the final semi-major, differentiating by final mass, and the initial semi-major axis placements at $e = 0$. In line with Chatterjee et al. (2008), planets that are scattered into orbits with high a tend to get high eccentricities. The same empty, wedge-shaped region pointed towards the placement of the initial middle planet can also been seen, which exists out of the requirement for orbital stability after scattering. Planets close to the initial placements tend to be from systems where a collision occurred, others are more scattered and from systems with ejection events. There is a clear difference between the semi-major axes of $1M_J$ and $2M_J$ planets close to the initial placements, arising from orbits mass dependence. For planets scattered to smaller distances, $a \simeq 1$ AU, the eccentricities vary widely. This decrease in e could be from long-term gravitational interactions between the inner and outer planet after scattering, in which the inner orbit circularizes.

A noteworthy part of this plot is the accumulation of planets with $5 < a < 20$ AU at $e \simeq 0.2$, the reason for which is not clear. From further examination we conclude that it is at least not in correlation with the final mass, nor the amount of planets left in the system. This accumulation and the subsequent 'gap' of planets with $\sim 0.2 < e <\sim 0.6$, is also reflected in figure 4.11, where the cumulative eccentricities of the changing radii sharply deviates from the observational line.

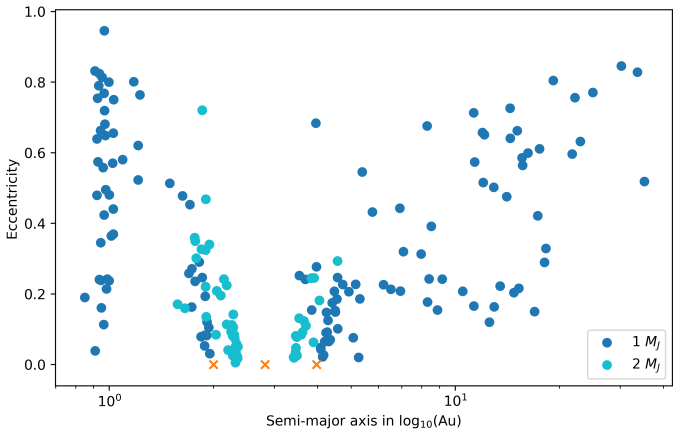

Figure 4.13: Final eccentricities and semi-major axes for planets in changing radii test, with color differentiating between $1M_J$ and $2M_J$ planets. Orange crosses marks the initial semi-major axes, with $e = 0$.

Chapter 5

Discussion & Conclusions

The purpose of this project was to investigate the effects of a contracting physical radius for young giant planets on planet scattering. Simulations of three equal-mass giant planets for the first 10^6 years of their development after gas had dissipated from the protoplanetary disk were conducted using `MERCURY`.

The sets of fixed radii planets show that the balance between collisions and ejections is indeed dependent on the radius. It shows that more collisions occur for larger planetary radii. The rate of ejections will also decrease for larger radii, however the total balance can not be properly analyzed since we expect more ejection to have occurred if the integration time had been extended beyond 10^6 years. For the set where the radii decreased with respect to time, the rate of collisions also increased, and the total number of planets lost in this way was similar to that of the fixed $2R_J$ simulations.

Collisions indeed occur quite early on in the evolution of the system compared to ejections, at which point the planetary radius can be a few times larger than at the very end. The Safronov number Θ, which depends on the planet radius and is shown in figure 4.9 for the contraction curve made in section 2.2.1. Θ increases as the planetary radius, and cross section becomes smaller, indicating the likelihood of collisions as an outcome of scattering is larger early on and diminishes over time.

In section 4.5 we noted the difference between the cumulative final eccentricity distribution between the fixed $2R_J$ set and the changing radii set (see figure 4.11), despite the similarity in rate of collisions and ejections. A KS-test confirmed that the eccentricities were not drawn from the same distribution, indicating that there might be another factor at play. The other measured difference between the sets were the occurrence times for collisions, seen in figure 4.6, where the first 3/4 of the collisions in the changing radii set occurred a factor of 3 times earlier at times when the radius was significantly greater than $2R_J$. This might suggest that the time dependence in the rate of collisions can have an effect on planetary orbital evolution. Further research into this could include more sets of fixed radii.

If a collision is the first type of event in our three planet systems in which a planet is lost, then the remaining planets will have unequal-masses. As reviewed in Davies et al. (2014), surviving planets of unequal-mass scattering will have smaller eccentricities compared to

equal-mass scattering. The resulting distribution of eccentricities then showed that systems with contracting planets did indeed have lower final eccentricities.

In comparison with observational data the performed integration set of dynamical radii planets had more planets with high eccentricities. This could perhaps be explained by initial planet masses being fixed and equal, and not drawn from some distribution, or the number of planets in each system only being three.

One possible improvement to these results would be increasing the number of systems in each simulated set. This could give greater statistical significance and allow for more conclusive results. Extending integration times could also give the opportunity to attain truer numbers for ejection-events, as there are likely to have been restrained by the low 10^6 years integration time.

The simulations in this thesis considered planets to be ejected at $a > 100$ AU. Although low, some justification for this could be for stars forming in dense stellar clusters where planets at such distances could instead get bounded to neighboring stars passing by. However that is not guaranteed to happen to all planets with large orbits and they can still play a part in the orbital evolution of remaining planets if still bound to the star. Thus it would be wise to use larger ejection distances for future simulations, perhaps on the order of $10^4 - 10^5$ AU similar to the outer edge distance of the Oort cloud[1].

How collisions were resolved for the simulations with changing radii in this thesis could be improved. Here the planets merged by combining the masses, but without any adjustment to the radius. Instead the radius continued to decrease from the same point on the contraction curve. One could expect that a collision between two giant planets could, beside fragmentation, also either significantly alter or reset the planet cooling and contraction.

The contraction curve used in this thesis may also be an upper limit for the effects of planet contraction on planet-planet scattering. It was created from the contraction curve from Baraffe et al. (2003), which is modeled based on the general theory of brown dwarf cooling. The difference between the formation processes of giant planets and brown dwarfs will affect initial conditions for cooling, brown dwarfs formed by direct collapse would be expected to be hotter than core accreted giant planets. Additionally, the metallicity can differ between the two, which in turn can influence the cooling and contraction. For example, Spiegel and Burrows (2012) present more complex cooling models of non-irradiated objects on the range of giant planets and small brown dwarfs. They give an analytical fit to the radii-mass-entropy relation, which could be interesting for further research into scattering outcomes for contracting planets in systems with diverse initial masses.

Acknowledgements

I am ever so grateful to my supervisor Dr. Alexander James Mustill, for his insight and helpful guidance throughout this work.

[1] https://solarsystem.nasa.gov/solar-system/oort-cloud/in-depth/ - Accessed: June 13th 2020

This project has been a solid anchor in a strange spring consisting of social distancing and self-isolation. I am never-the-less very thankful for to my fellow bachelor students for their useful advice and the fruitful discussions we've been able to have, despite the circumstances.

Lastly, I want to express my deep appreciation for the support I have received from family and friends.

Bibliography

P. J. Armitage. Lecture notes on the formation and early evolution of planetary systems. *arXiv e-prints*, art. astro-ph/0701485, Jan. 2007.

I. Baraffe, G. Chabrier, T. S. Barman, F. Allard, and P. H. Hauschildt. Evolutionary models for cool brown dwarfs and extrasolar giant planets. The case of HD 209458. *A&A*, 402:701–712, May 2003. doi: 10.1051/0004-6361:20030252.

J. E. Chambers. A hybrid symplectic integrator that permits close encounters between massive bodies. *MNRAS*, 304(4):793–799, Apr. 1999. doi: 10.1046/j.1365-8711.1999.02379.x.

J. E. Chambers, G. W. Wetherill, and A. P. Boss. The Stability of Multi-Planet Systems. *Icarus*, 119(2):261–268, Feb. 1996. doi: 10.1006/icar.1996.0019.

S. Chatterjee, E. B. Ford, S. Matsumura, and F. A. Rasio. Dynamical Outcomes of Planet-Planet Scattering. *ApJ*, 686(1):580–602, Oct. 2008. doi: 10.1086/590227.

M. B. Davies, F. C. Adams, P. Armitage, J. Chambers, E. Ford, A. Morbidelli, S. N. Raymond, and D. Veras. The Long-Term Dynamical Evolution of Planetary Systems. In H. Beuther, R. S. Klessen, C. P. Dullemond, and T. Henning, editors, *Protostars and Planets VI*, page 787, Jan. 2014. doi: 10.2458/azu_uapress_9780816531240-ch034.

M. R. Hogerheijde. *Protoplanetary Disk*, pages 1357–1366. Springer Berlin Heidelberg, Berlin, Heidelberg, 2011. ISBN 978-3-642-11274-4. doi: 10.1007/978-3-642-11274-4_1299. URL `https://doi.org/10.1007/978-3-642-11274-4_1299`.

S. Ida and J. Makino. N-Body simulation of gravitational interaction between planetesimals and a protoplanet . I. velocity distribution of planetesimals. *Icarus*, 96(1):107–120, Mar. 1992. doi: 10.1016/0019-1035(92)90008-U.

M. Jurić and S. Tremaine. Dynamical Origin of Extrasolar Planet Eccentricity Distribution. *ApJ*, 686(1):603–620, Oct. 2008. doi: 10.1086/590047.

M. Mayor and D. Queloz. A Jupiter-mass companion to a solar-type star. *Nature*, 378 (6555):355–359, Nov. 1995. doi: 10.1038/378355a0.

W. H. Press, S. A. Teukolsky, W. T. Vetterling, and B. P. Flannery. *Numerical recipes in FORTRAN. The art of scientific computing*. 1992.

D. A. Rothery, I. Gilmour, and M. A. Sephton. *An Introduction to Astrobiology (3rd ed.)*. 2018.

D. S. Spiegel and A. Burrows. Spectral and Photometric Diagnostics of Giant Planet Formation Scenarios. *ApJ*, 745(2):174, Feb. 2012. doi: 10.1088/0004-637X/745/2/174.

Wikimedia Commons. Digram illustrating and explaining various terms in relation to orbits of celestial bodies, 2007. URL `https://commons.wikimedia.org/wiki/File:Orbit1.svg`. File: `Orbit1.svg`.

J. N. Winn and D. C. Fabrycky. The Occurrence and Architecture of Exoplanetary Systems. *ARA&A*, 53:409--447, Aug. 2015. doi: 10.1146/annurev-astro-082214-122246.

A. Wolszczan and D. A. Frail. A planetary system around the millisecond pulsar PSR1257 + 12. *Nature*, 355(6356):145--147, Jan. 1992. doi: 10.1038/355145a0.